Proton Transfer Voltammetry at Electrodes Modified with Acid Thiol Monolayers

ARTICLE *in* ANALYTICAL CHEMISTRY · JUNE 2012

Impact Factor: 5.64 · DOI: 10.1021/ac301040r · Source: PubMed

analytical chemistry

Article

pubs.acs.org/ac

Proton Transfer Voltammetry at Electrodes Modified with Acid Thiol Monolayers

Antonio M. Luque,[†] Willem H. Mulder,[‡] Juan José Calvente,[†] Angel Cuesta,[§] and Rafael Andreu*[,†]

[†]Departamento de Química Física, Universidad de Sevilla, 41012-Sevilla, Spain

[‡]Department of Chemistry, University of the West Indies, Mona Campus, Kingston 7, Jamaica

[§]Instituto de Química Física "Rocasolano", CSIC, 28006-Madrid, Spain

Supporting Information

ABSTRACT: By combining a description of the potential profile at electrodes coated with acid thiol monolayers with a quadratic relationship between activation energy and electrode potential, a rather simple expression for proton transfer voltammograms is derived. Our electrostatic analysis shows that proton transfer can only produce narrow voltammetric peaks when the immobilized acid groups lie close to the metal substrate. Quantitative fits of experimental voltammograms obtained with an Au(111) electrode modified with a 11-mercaptoundecanoic monolayer at pH 8.5 reveal that less than 1% of the carboxylic groups in the monolayer participate in the potential induced proton transfer process and that these groups lay close to the metal surface. A preliminary analysis of the kinetic parameters suggests that the interfacial electric field facilitates an intrinsically slow proton exchange between a proton donor and acceptor pair that are not in close contact with each other at the interface.

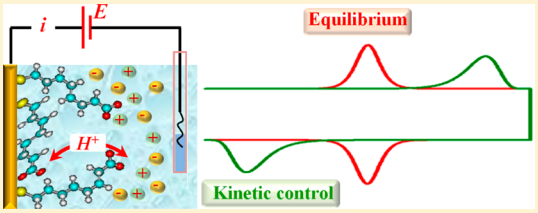

Self-assembly of thiols offers a convenient route to impart predesigned functionalities to metal surfaces.[1] These thiol modified surfaces have found applications in a variety of fields, such as molecular electronics,[2] cell adhesion,[3] and biosensing.[4] Particularly, monolayers that expose carboxylic groups toward an external solution constitute useful platforms for electrostatic and covalent immobilization of proteins.[5] Regardless of their popularity, some fundamental aspects of mercaptoalkanoic acid monolayers, like their extent of ionization at a given pH, remain poorly understood. Thus, reported pK_a values for 11-mercaptoundecanoic acid (MUA) monolayers deposited on gold vary from 4.5 to 10.3.[6−12] Some of these differences may be due to limitations of the sampling technique, but they are also likely to reflect some intrinsic complexities of these systems, as illustrated by the coexistence of two populations of carboxylic groups with different pK_a values in an alkanoic acid monolayer anchored on a silicon support.[13]

Electrochemical techniques have been used to monitor changes in the ionization state of these monolayers brought about by acid/base interactions with the solution components.[9,11,14−16] The next step, from a conceptual point of view, was to take advantage of the electrochemical control over the applied potential to electrostatically induce the proton transfer between the monolayer and the solution. White at al.[17] were the first to report reversible voltammetric waves associated with the protonation/deprotonation of mixed monolayers of MUA and decanethiol deposited on Ag(111). Similar voltammetric responses were obtained later for MUA,[18] 4-mercaptobenzoic acid,[19] and 3-mercaptopropylphosphonic acid[20] monolayers deposited on polycrystalline gold surfaces.

Early attempts[21−23] to provide a theoretical description of potential induced proton transfer at the monolayer/solution interface were restricted to equilibrium conditions and were based on an electrostatic analysis of the interfacial potential profile. More recently, Lennox et al.[18] adopted a Butler−Volmer type formalism to describe the influence of the applied potential on the kinetics of proton transfer and derived an expression for the protonation/deprotonation impedance. Notwithstanding a satisfactory fit of the impedance dependence on frequency, the number of parameters and the empirical nature of their approach prevented a satisfactory interpretation in terms of equivalent circuit elements.

While adopting an average potential description of the interfacial potential profile, our electrostatic approach removes two assumptions that were present in previous models. First, we do not require that all the thiol molecules adopt the same orientational conformation. It should be noted that crystallographic order, typical of alkanethiol monolayers in vacuum,[24] disappears as soon as the monolayer is brought into contact with a liquid phase.[25] In the case of ω-mercaptoalkanoic monolayers, this hypothesis is supported by the convergence of the potentials of zero charge of Au(111) electrodes modified with 3-mercaptopropionic acid, 6-mercaptohexanoic acid, and MUA monolayers for pH $\geq$ 9 to a value that is independent of the molecular chain length.[9] Recent molecular dynamics simulations of carboxylic-acid terminated self-assembled monolayers have reached the same conclusion regarding the

Received: April 30, 2012
Accepted: June 5, 2012
Published: June 5, 2012

   dx.doi.org/10.1021/ac301040r | *Anal. Chem.* 2012, 84, 5778−5786

presence of the conformational disorder in these systems.[26] Second, we do not assume that all the carboxylic groups in the monolayer are involved in the potential induced proton transfer. Since reversible voltammograms are observed at pH ~ 9, where most carboxylic groups directly exposed to the solution should be ionized,[6−12] it seems likely that only carboxylic groups that are surrounded by a specific environment (e.g., those that are buried within a disordered monolayer) may retain their ability to switch between their protonated and deprotonated forms under the influence of the applied potential. Therefore, we assume the presence of two populations of acid groups in the monolayer, those whose degree of ionization is determined exclusively by the solution pH and those that are influenced also by the electrode potential.

As in the case of electrochemical electron transfer, the electrode potential modifies also the standard free energy difference (ΔG^0) between reactants and products for a proton transfer reaction. The electrostatic model of the interface provides an explicit relationship between the electrode potential and ΔG^0, but an assumption on the proton transfer mechanism is required to further relate ΔG^0 and the activation free energy ($\Delta G^{\ddagger}$). Modern theories of proton transfer in solution emphasize the role of the environmental reorganization in determining the activation free energy.[27−29] Depending on whether a strong or a weak hydrogen bond between proton donor and acceptor is formed in the reactant complex, the proton transfer regime is classified as adiabatic or nonadiabatic, respectively.[30] In both cases, a quadratic relationship between $\Delta G^{\ddagger}$ and ΔG^0 has been derived, though the physical meaning of the second order polynomial coefficients is different in each case.[31,32] In the absence of a detailed microscopic characterization of our system, we have assumed that proton donor and acceptor are not in close contact and that the potential-induced proton transfer takes place according to a nonadiabatic mechanism. Under these circumstances, the $\Delta G^{\ddagger}$ vs ΔG^0 relationship becomes formally identical to the classical Marcus expression for homogeneous electron transfer.

On the basis of the above assumptions, we have derived an implicit expression to compute proton transfer voltammograms. Application of this expression requires knowledge of the values of the system parameters that determine the potential profile at the modified electrode surface. However, we have shown that this prerequisite can be avoided under conditions that apply to experimental voltammograms so that a much simpler expression (analogous to that of surface redox voltammograms) can be used to compare theory and experiment. A preliminary assessment of voltammograms recorded with a MUA-modified Au(111) electrode showed that satisfactory quantitative fits are obtained by assuming that only a small fraction (~1%) of the carboxylic groups in the monolayer are involved in the potential-induced proton transfer and that these groups lie close to the metal surface.

THEORY

Electrostatic Model. We consider the potential distribution in the vicinity of a gold electrode modified with a thiol monolayer exhibiting acid/base properties, as depicted in Figure 1A for the case of an ordered ω-mercaptoalkanoic acid monolayer. The monolayer contains $\Gamma_T^{p/dp}$ moles of ionizable acid/base groups per unit area and may also contain nonionizable molecules of similar structure. The undissociated carboxylic (R-OH) and ionized carboxylate ($R\text{-}O^-$) groups are

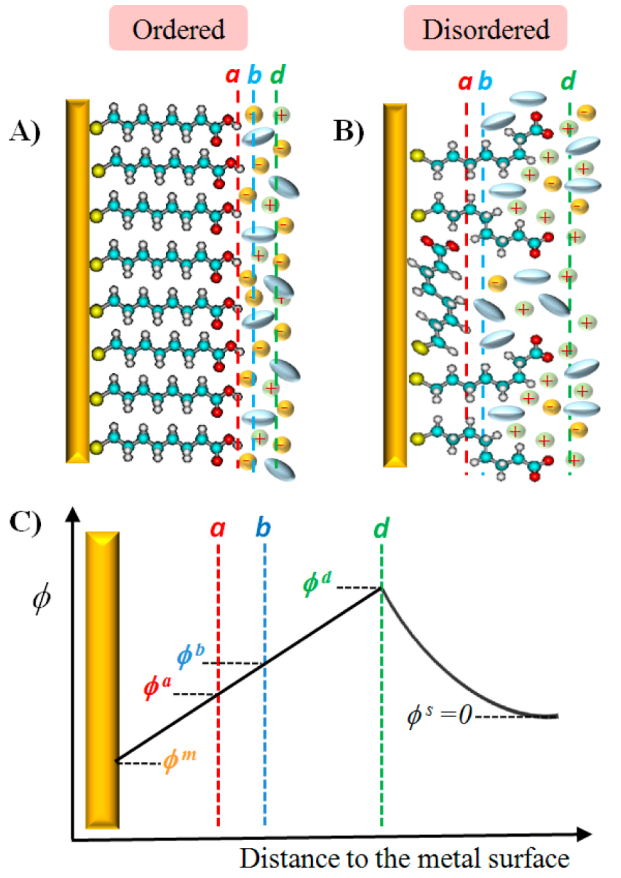

Figure 1. Schematic representation of a gold electrode modified with an (A) ordered or (B) disordered ω-mercaptoalkanoic acid monolayer, which is in contact with an aqueous electrolyte solution. (C) Potential profile across the modified electrode surface, indicating the location of the *a*, *b*, and *d* planes. In the case of the disordered monolayer, labels *a* and *b* indicate just one possible choice for the location of the proton transfer planes.

initially assumed to be located at a plane *a*, parallel to the electrode surface. The proton exchange process involves also a proton acceptor (OH^-) and a proton donor (H_2O) from solution, which share a common plane *b* of closest approach to the electrode surface (see parts A and C of Figure 1). Other electrolyte ions are allowed to approach the electrode up to plane *d* only, thereby defining a dielectric layer between metal and solution that includes both the thiol monolayer and its solvation sheath, and it is characterized by an integral capacity K_{md}. Thus, proton transfer involves a proton moving between planes *a* and *b*. The average potential values at these two planes, ϕ^a and ϕ^b, with respect to the bulk solution ($\phi^s = 0$) can be expressed in terms of the electrode potential ϕ^m, according to

$$\phi^a = \phi^d + \omega_a(\phi^m - \phi^d) \quad (1)$$

where ϕ^d is the potential drop across the diffuse layer and $\omega_a = K_{md}/K_{ad}$ is the ratio between the integral capacity of the solvated monolayer and that of the dielectric slab limited by plane *a* and the diffuse layer boundary *d*, so that $0 < \omega_a < 1$.

Thus, when the proton transfer takes place in the outer part of a well ordered monolayer, as illustrated in Figure 1A, ω_a will adopt a low value (~0.1) that is expected to increase upon decreasing the thiol chain length. In the case of a disordered monolayer, as illustrated in Figure 1B, a continuous distribution

dx.doi.org/10.1021/ac301040r | Anal. Chem. 2012, 84, 5778−5786

of plane a locations and ω_a values can be envisaged. Particularly, high ω_a values (~0.9), which are independent of the thiol chain length, can be expected for molecular orientations of the adsorbed thiol whose plane a lays close to the metal surface. Analogously,

$$\phi^b = \phi^d + \omega_b(\phi^m - \phi^d) \quad (2)$$

where $\omega_b = K_{md}/K_{bd}$.

As deprotonation proceeds, new charges are generated at plane a, and ϕ^a and ϕ^b deviate progressively from the values predicted by eqs 1 and 2. However, to keep the mathematical problem more tractable, we will still keep this approximate potential profile to derive analytical expressions describing the protonation/deprotonation process. As explained in the Supporting Information, this approximation limits the validity of our approach to low $\Gamma_T^{p/dp}$ values.

As previously reported,[6−12] some ionization of the surface attached carboxylic groups takes place whenever these monolayers contact aqueous solutions with pH > 4. These partially ionized monolayers develop a stronger affinity for water molecules and display repulsive electrostatic interactions between ionized groups. Both effects are expected to induce orientational disorder within the organic film. Under these circumstances, some thiol molecules are likely to adopt new spatial orientations that bring their carboxylic groups closer to the electrode surface (see Figure 1B). These buried acid groups are expected to display distinct pK_a values, due to their new environment, and become more sensitive toward changes in the applied electrode potential (see the Results and Discussion). In the absence of detailed information on the space charge distribution of the carboxylates that are exposed to the solution, the surface concentration of which is denoted by $\Gamma^{ext}_{R\text{-}O^-}$, the electrostatic influence of these external charges on the dissociation of the buried acid groups is modeled by simply assuming that their charge density, $q^{ext}_{R\text{-}O^-} = -F \cdot \Gamma^{ext}_{R\text{-}O^-}$, is located at plane d. Except for this additional charge contribution, the electrostatic model describing proton transfer of buried acid groups coincides with that previously outlined for proton transfer involving solution exposed acid groups at well ordered monolayers.

Proton Transfer at Equilibrium. The equilibrium condition for the overall reaction

$$\text{R-OH(plane } a) + \text{OH}^-\text{(sol)} \rightleftarrows \text{R-O}^-\text{(plane } a) + \text{H}_2\text{O(sol)} \quad (3)$$

can be expressed in terms of the electrochemical potentials of the participating species as

$$\mu^{0,a}_{R\text{-OH}} + RT \ln \theta_{R\text{-OH}} + \mu^{0,sol}_{OH^-} + RT \ln a^{sol}_{OH^-} = \mu^{0,a}_{R\text{-O}^-} + RT \ln \theta_{R\text{-O}^-} - F\phi^a + \mu^{0,sol}_{H_2O} \quad (4)$$

where $\theta_i = \Gamma_i/\Gamma_T^{p/dp}$ is the fraction of either carboxylic ($i \equiv$ R-OH) or carboxylate ($i \equiv$ R-O$^-$) groups within the population of thiols that undergo a potential-induced proton exchange. This expression shows that, under equilibrium conditions, the value of the degree of surface dissociation $\theta_{R\text{-}O^-}$ depends on the applied electrode potential ϕ^m via eq 1. This relationship can be made explicit by combining eqs 1 and 4 to obtain

$$\phi^m = \frac{\omega_a - 1}{\omega_a}\phi^d + \frac{1}{\omega_a}\left(\frac{\Delta G^0}{F} + \frac{RT}{F}\ln\frac{\theta_{R\text{-}O^-}}{\theta_{R\text{-OH}}a^{sol}_{OH^-}}\right) \quad (5)$$

with $\Delta G^0 = \mu^{0,a}_{R\text{-}O^-} + \mu^{0,sol}_{H_2O} - \mu^{0,a}_{R\text{-OH}} - \mu^{0,sol}_{OH^-}$. We can define a half-conversion potential $\phi^m_{1/2}$ as the equilibrium potential where $\theta_{R\text{-}O^-} = \theta_{R\text{-OH}}$, so that

$$\phi^m_{1/2} = \frac{\omega_a - 1}{\omega_a}\phi^d_{1/2} + \frac{1}{\omega_a}\left(\frac{\Delta G^0}{F} + \frac{RT}{F}\ln\frac{1}{a^{sol}_{OH^-}}\right) \quad (6)$$

Therefore, $\phi^m_{1/2}$ is predicted to shift with the solution pH at a rate that depends on the value of ω_a^{-1}. Equations 5 and 6 can be combined to give

$$\phi^m = \phi^m_{1/2} + \frac{\omega_a - 1}{\omega_a}(\phi^d - \phi^d_{1/2}) + \frac{RT}{\omega_a F}\ln\frac{\theta_{R\text{-}O^-}}{1 - \theta_{R\text{-}O^-}} \quad (7)$$

Except for the second term on the right-hand side, which can be considered as a diffuse layer perturbation term, this expression coincides with the equilibrium condition for a surface immobilized redox couple, where the number of electrons n has been replaced by ω_a.[33]

Rates of Protonation and Deprotonation. The rates of protonation/deprotonation (r_p/r_{dp}) can be expressed in terms of the respective rate constants (k_p/k_{dp}) and activation free energies ($\Delta G^‡_p/\Delta G^‡_{dp}$) as follows

$$r_p = k_p\theta_{R\text{-}O^-} = Ze^{-\Delta G^‡_p/RT}\theta_{R\text{-}O^-} \quad (8)$$

$$r_{dp} = k_{dp}\theta_{R\text{-OH}}c^{sol}_{OH^-} = Ze^{-\Delta G^‡_{dp}/RT}\theta_{R\text{-OH}}c^{sol}_{OH^-} \quad (9)$$

where Z is a frequency factor and $c^{sol}_{OH^-}$ the bulk concentration of OH$^-$. Activation free energies, containing the effect of electrode potential ϕ^m among others, are described by the following relationship:[27,28]

$$\Delta G^‡_{dp,p} = w_{dp,p} + \frac{(\lambda \pm \Delta G^0_{ab})^2}{4\lambda} \quad (10)$$

where λ is the reorganization free energy. The positive sign applies in the case of deprotonation of the carboxylic group, and w_{dp} is the average work involved in bringing the OH$^-$ ion to a distance b from the electrode surface, while the carboxylic group is fixed at a distance a. This work term can be written as the sum of a nonelectrostatic term $g^b_{OH^-}$ and an electrostatic contribution $-F\phi^b$. The negative sign in eq 10 and work w_p of carrying a water molecule from bulk solution to plane b pertain to the protonation step, which includes only a nonelectrostatic work term $g^b_{H_2O}$. Once the encounter complex with reactants at planes a and b has been formed, the standard free energy change that accompanies deprotonation to give products at the same locations is

$$\Delta G^0_{ab} = \mu^{0,a}_{R\text{-}O^-} + \mu^{0,sol}_{H_2O} + g^b_{H_2O} - \mu^{0,a}_{R\text{-OH}} - \mu^{0,sol}_{OH^-} - g^b_{OH^-} - F(\phi^a - \phi^b) \quad (11)$$

The last term, $-F(\phi^a - \phi^b) = -F(\omega_a - \omega_b)(\phi^m - \phi^d)$, describes most of the effect of electrode potential on the protonation/deprotonation rates. Further algebraic manipulations are facilitated by recasting eq 11 into the following abbreviated form:

$$\Delta G^0_{ab} = \gamma + \beta(\phi^m - \phi^d) \quad (12)$$

with $\gamma = \mu^{0,a}_{R\text{-}O^-} + \mu^{0,sol}_{H_2O} + g^b_{H_2O} - \mu^{0,a}_{R\text{-OH}} - \mu^{0,sol}_{OH^-} - g^b_{OH^-}$ and $\beta = -F(\omega_a - \omega_b)$. An additional relationship between γ and β can

dx.doi.org/10.1021/ac301040r | Anal. Chem. 2012, 84, 5778−5786

be derived from the equality of r_p and r_{dp} at $\phi^m{}_{1/2}$, under equilibrium conditions, to give

$$\gamma = w_{p,1/2} - w_{dp,1/2} + RT \ln c^{sol}_{OH^-} - \beta(\phi^m_{1/2} - \phi^d_{1/2}) \quad (13)$$

and hence, with the shorthand notation $\Delta w_{1/2} = w_{p,1/2} - w_{dp,1/2} + RT \ln c^{sol}_{OH^-}$,

$$\Delta G^0_{ab} = \Delta w_{1/2} + \beta(E^c - E^c_{1/2}) \quad (14)$$

where $E^c = \phi^m - \phi^d$ is the electrode potential corrected for the diffuse layer potential.

Explicit expressions for the effect of the applied potential on k_p and k_{dp} can now be obtained by combining eqs 8−10 and 14 to give

$$\ln k_p = \ln k^{ap}_s - \frac{\alpha^{ap}_p F}{RT}(E^c - E^c_{1/2}) - \frac{\alpha_M F^2}{R^2T^2}(E^c - E^c_{1/2})^2 \quad (15)$$

$$\ln(k_{dp} c^{sol}_{OH^-}) = \ln k^{ap}_s + \frac{F(\phi^d - \phi^d_{1/2})}{RT} + \frac{\alpha^{ap}_{dp} F}{RT}(E^c - E^c_{1/2}) - \frac{\alpha_M F^2}{R^2T^2}(E^c - E^c_{1/2})^2 \quad (16)$$

where

$$\ln k^{ap}_s = \ln Z - \frac{\lambda}{4RT} + \frac{1}{2}\ln c^{sol}_{OH^-} - \frac{w_{p,1/2} + w_{dp,1/2}}{2RT} - \frac{\Delta w^2_{1/2}}{4\lambda RT} \quad (17)$$

$$\alpha^{ap}_p = \frac{\omega_a - \omega_b}{2}\left(1 - \frac{\Delta w_{1/2}}{\lambda}\right) \quad (18)$$

$$\alpha^{ap}_{dp} = \frac{\omega_a + \omega_b}{2} + \frac{\omega_a - \omega_b}{2}\cdot\frac{\Delta w_{1/2}}{\lambda} \quad (19)$$

and

$$\alpha_M = \frac{(\omega_a - \omega_b)^2 RT}{4\lambda} \quad (20)$$

It is interesting to note that the α^{ap}_p and α^{ap}_{dp} values are related by the simple relationship

$$\alpha^{ap}_p + \alpha^{ap}_{dp} = \omega_a \quad (21)$$

Voltammetric Response. As stated before, scanning the electrode potential can trigger the proton transfer, producing a flow of non-faradaic current through the external circuit and leads to the observation of protonation/deprotonation voltammetric peaks.

The non-faradaic current density i stems from a change in the charge density of the electrode surface q^m, which satisfies the electroneutrality condition at the interface:

$$q^m = -q^d + F\Gamma^{p/dp}_T \theta_{R\text{-}O^-} + F\Gamma^{ext}_{R\text{-}O^-} \quad (22)$$

where $\Gamma^{ext}_{R\text{-}O^-}$ is assumed to be determined by the solution pH and to be independent of the electrode potential, and q^d is the charge density of the diffuse layer. By taking derivatives with respect to time, the following expression is derived for the charging/discharging current density (see the Supporting Information):

$$i = \frac{dq^m}{dt} = \frac{C_d}{1 + C_d K^{-1}_{md}} v + \frac{(1 + C_d K^{-1}_{ad}) F\Gamma^{p/dp}_T}{1 + C_d K^{-1}_{md}} \frac{d\theta_{R\text{-}O^-}}{dt} \quad (23)$$

where $v = d\phi^m/dt$ is the potential scan rate, C_d is the diffuse layer capacity, and $d\theta_{R\text{-}O^-}/dt$ is given by

$$\frac{d\theta_{R\text{-}O^-}}{dt} = k_{dp} c^{sol}_{OH^-}(1 - \theta_{R\text{-}O^-}) - k_p \theta_{R\text{-}O^-} \quad (24)$$

whose numerical resolution is described in the Supporting Information.

RESULTS AND DISCUSSION

Proton Transfer in Equilibrium. Whenever the protonation/deprotonation process is fast enough, so that eq 5 applies, the deprotonation rate can be formulated as

$$\left(\frac{d\theta_{R\text{-}O^-}}{dt}\right)_{eq} = \frac{d\theta_{R\text{-}O^-}}{d\phi^m}\cdot v \quad (25)$$

Equation 7 provides an explicit relationship between $\theta_{R\text{-}O^-}$ and ϕ^m which leads to

$$\frac{d\theta_{R\text{-}O^-}}{d\phi^m} = \left[\frac{\omega_a - 1}{\omega_a}\frac{d\phi^d}{d\theta_{R\text{-}O^-}} + \frac{RT}{\omega_a F} \times \frac{(1 + \exp(\omega_a\varphi)\exp((1 - \omega_a)\varphi^d))^2}{\exp(\omega_a\varphi)\exp((1 - \omega_a)\varphi^d)}\right]^{-1} \quad (26)$$

where $\varphi = F(\phi^m - \phi^m_{1/2})/RT$ and $\varphi^d = F(\phi^d - \phi^d_{1/2})/RT$. When the diffuse layer perturbation can be neglected, so that $d\phi^d/d\theta_{R\text{-}O^-} \approx 0$, $\varphi^d \approx 0$, and $C_d \gg K_{md}, K_{ad}$, eqs 23, 25, and 26 can be combined to obtain

$$i = K_{md} v + \frac{\omega_a{}^2 F^2}{RT}\frac{v\Gamma^{p/dp}_T \exp(\omega_a\varphi)}{(1 + \exp(\omega_a\varphi))^2} \quad (27)$$

which is identical to the expression for a surface redox couple,[33] where n has been replaced by ω_a and, by analogy, we can expect for the protonation/deprotonation case bell shaped voltammetric waves, which display a maximum at $\phi^m = \phi^m_{1/2}$, whose height increases with $\Gamma^{p/dp}_T$ and whose width decreases upon increasing ω_a. Moreover, the dependence on the solution pH is mainly contained in the value of $\phi^m_{1/2}$ (see eq 6) so that voltammetric waves are expected to retain their overall shape and shift at a rate of $(60/\omega_a)$ mV per pH unit at 298 K as the solution pH is being changed.

Figure 2 illustrates the influence of $\Gamma^{p/dp}_T$ and ω_a on the voltammetric wave shape, under conditions where the protonation process remains in equilibrium. The most striking feature is the absence of noticeable voltammetric peaks when the acid groups are located in the vicinity of the outer Helmholtz plane, so that $\omega_a \sim 0$.

As ω_a decreases, the degree of protonation of the monolayer becomes less sensitive to changes in the applied potential, and the derivative $d\theta_{R\text{-}O^-}/d\phi^m$ becomes too small (see lower panels in Figure 2) to generate a significant current flow through the external circuit. The minimum ω_a value that leads to noticeable voltammetric peaks can be set at ~0.3. On the other hand, well developed peaks, with half-height widths close to 90 mV at 298 K, are obtained when $\omega_a \to 1$.

It is interesting to note that, in the presence of a high surface concentration of ionizable groups (right panels of Figure 2),

dx.doi.org/10.1021/ac301040r | Anal. Chem. 2012, 84, 5778−5786

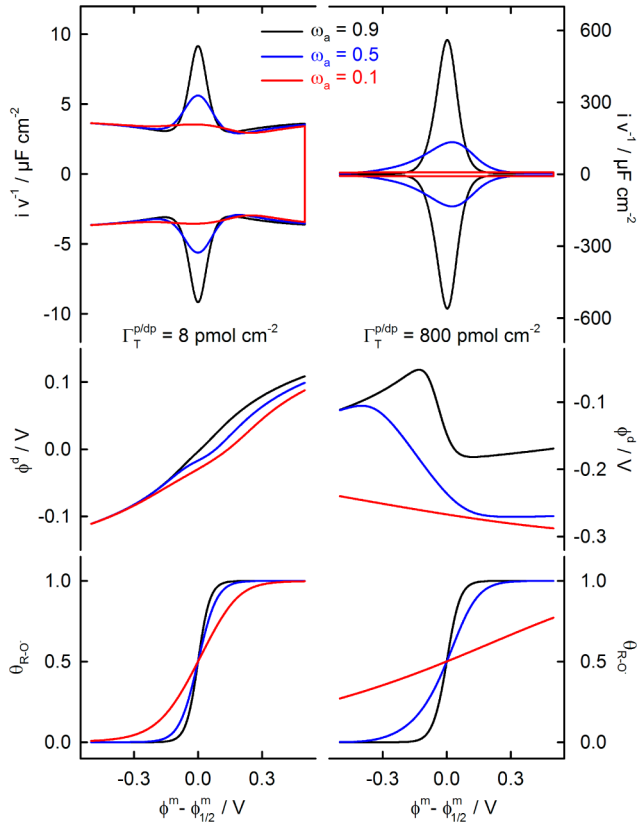

Figure 2. Protonation/deprotonation cyclic voltammograms (upper panels), diffuse layer potential (middle panels), and deprotonation degree of the monolayer (lower panels) computed for the indicated values of ω_a and $\Gamma_T^{p/dp}$ under equilibrium conditions. Other parameter values: $c_{elect} = 10^{-3}$ M, $K_{md} = 4.1$ μF cm^{-2}, $\phi^m_{1/2} = \phi^m_{pzc} = 0$, $q^{ext}_{R\text{-}O^-} = 0$, $T = 298$ K.

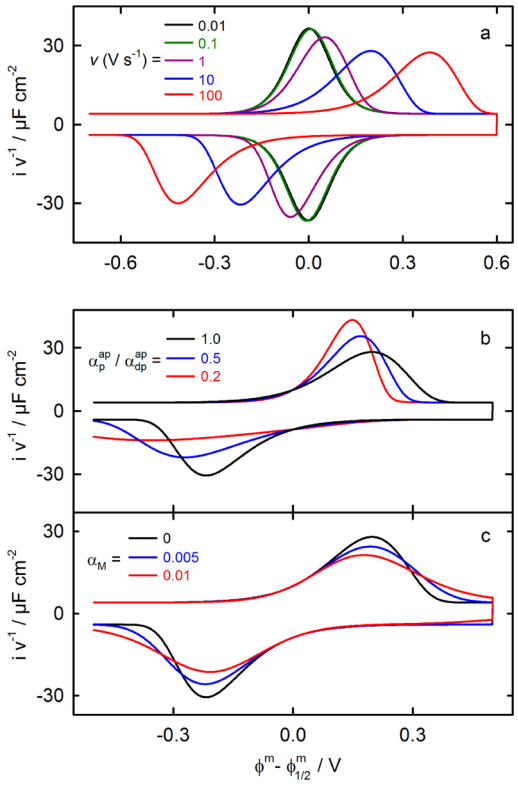

Figure 3. . Protonation/deprotonation cyclic voltammograms under kinetic control. Influence of (a) scan rate v for $\alpha_p^{ap} = 0.3$, $\alpha_M = 0$, (b) the $\alpha_p^{ap}/\alpha_{dp}^{ap}$ ratio for $\alpha_M = 0$, $v = 10$ V s^{-1}, and (c) the quadratic potential term α_M for $\alpha_p^{ap} = 0.3$, $v = 10$ V s^{-1}. Other parameter values: $\omega_a = 0.6$, $\Gamma_T^{p/dp} = 10^{-10}$ mol cm^{-2}, $c_{elec} = 1$ M, $K_{md} = 4.1$ μF cm^{-2}, $\phi^m_{1/2} = \phi^m_{pzc} = 0$, $k_s^{ap} = 10$ s^{-1}, $q^{ext}_{R\text{-}O^-} = 0$, $T = 298$ K.

diffuse layer potentials remain negative for $\phi^m > \phi^m_{pzc}$, and their changes parallel those of the degree of protonation. On the other hand, when the surface concentration of ionizable groups is low (left panels of Figure 2), diffuse layer potentials change their sign in the vicinity of the pzc and do not bear an obvious correspondence with the protonation process. The presence of diffuse layer perturbation terms suggests that both the electrolyte concentration and potential of zero charge should affect the voltammetric response. However, as long as we restrict ourselves to a reasonable range of parameter values: $\omega_a \geq 0.3$, 10^{-3} M $\leq c_{elect} \leq 1$ M, and -0.5 V $\leq \phi^m_{1/2} - \phi^m_{pzc} \leq 0.5$ V, c_{elect} and ϕ^m_{pzc} mostly affect the background capacitive current and, only to a lesser extent, the height/width aspect ratio of the voltammetric waves.

Kinetic Control of Proton Transfer. Cyclic voltammograms computed under equilibrium conditions display positive and negative waves that are symmetrical with respect to the potential axis. This symmetry, and the underlying protonation equilibrium, can be broken by increasing the scan rate. Once the time scale of the voltage scan (RT/Fv) approaches the protonation/deprotonation time scale ($1/k_s^{ap}$), the degree of protonation at each potential lags behind its equilibrium value and both voltammetric peaks develop at finite overpotentials with respect to $\phi^m_{1/2}$ (Figure 3a).

The rates of protonation and deprotonation at each potential, and therefore the voltammetric response, are largely determined by eqs 15 and 16. Apart from the diffuse layer correction terms, which we will consider later, the dependence of the rate constants on the applied potential E can formally be described as a combination of Butler–Volmer kinetics plus a quadratic term, with charge transfer coefficients α_p^{ap}, α_{dp}^{ap}, and α_M defined in eqs 18–20. Familiar voltammetric behavior (Figure 3a) is obtained when (a) $\alpha_M = 0$, in which case the quadratic potential terms vanish, (b) the electrolyte concentration is high, implying that $\phi^d - \phi^d_{1/2} \approx 0$, and (c) $\alpha_p^{ap} = \alpha_{dp}^{ap}$, so that positive and negative waves have the same height. The onset of the kinetic control leads to a peak separation that increases with v (i.e., to trumpet plots) and to lower less symmetric voltammetric waves, much as in the case of a slow surface redox process.

Only when $\alpha_{dp}^{ap} = \alpha_p^{ap} = \omega_a/2$, can we expect positive and negative waves to possess the same height and undergo the same potential shift upon increasing the scan rate. Keeping in mind that $\alpha_{dp}^{ap} + \alpha_p^{ap} = \omega_a$, a deprotonation transfer coefficient α_{dp}^{ap} larger than $\omega_a/2$ implies that the positive (negative) wave becomes narrower (wider) and develops at lower (higher) overpotentials (see Figure 3b), since now k_{dp} varies more rapidly and k_p more slowly with the applied potential. Further wave-shape changes are brought about by the quadratic potential term in eqs 15 and 16, which produces a decrease of both rate constants k_{dp} and k_p as the magnitude of the overpotential is increased. Figure 3c illustrates how a stronger influence of the quadratic term, or a higher value of α_M, results in a progressive flattening of the voltammetric waves.

The presence of a diffuse layer potential drop ϕ^d may also modify the voltammetric wave-shape in the presence of low electrolyte concentrations, as illustrated in Figure 4. To assess

dx.doi.org/10.1021/ac301040r | Anal. Chem. 2012, 84, 5778–5786

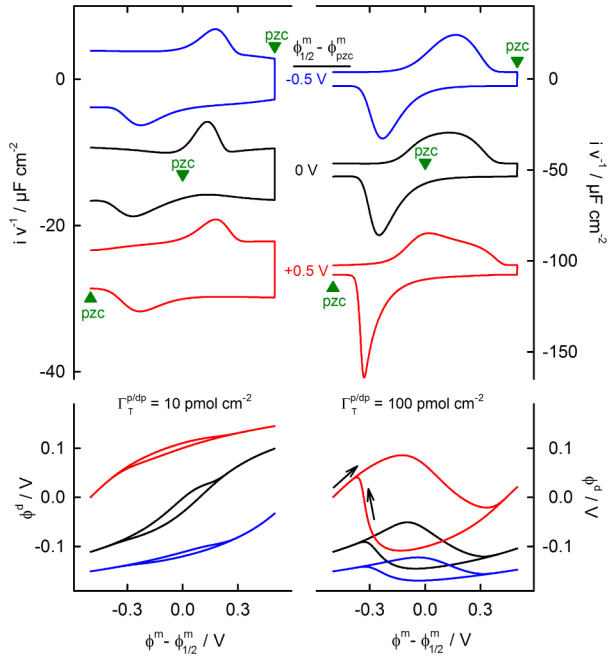

Figure 4. Protonation/deprotonation cyclic voltammograms (upper panels) and diffuse layer potential (lower panels) computed for the indicated values of $\Gamma_T^{p/dp}$ and $\phi^m_{1/2} - \phi^m_{pzc}$. Other parameter values: ω_a = 0.6, $\alpha_p^{ap} = \alpha_{dp}^{ap}$, α_M = 0, $c_{elect} = 10^{-3}$ M, K_{md} = 4.1 μF cm^{-2}, ν = 10 V s^{-1}, k_s^{ap} = 10 s^{-1}, $q^{ext}_{R\text{-}O^-}$ = 0, T = 298 K. Black arrows in the lower panels indicate the scan direction.

the influence of the diffuse layer term, it is convenient to consider two limits, depending on whether ϕ^d closely follows the expected values for a neutral monolayer (case of low $\Gamma_T^{p/dp}$, as depicted in the left panels of Figure 4), or whether ϕ^d exhibits a marked hysteresis along the cyclic voltammogram due to the slow protonation/deprotonation of the acid groups (case of high $\Gamma_T^{p/dp}$, as depicted in the right panels of Figure 4).

In relation to the low $\Gamma_T^{p/dp}$ case, it may be observed from Figure 4 that the positive peak is narrower than its negative counterpart, even when $\alpha_{dp}^{ap} = \alpha_p^{ap}$. The origin of this effect can be traced to the electrostatic work required to bring the OH^- anion in contact with the monolayer, which translates into somewhat different expressions relating k_{dp} and k_p with ϕ^d. Thus, from eqs 15 and 16, with α_M = 0 and at a given $\phi^m - \phi^m_{1/2}$, one obtains

$$\ln k_p \propto \frac{\alpha_p^{ap} F}{RT}(\phi^d - \phi^d_{1/2}) \quad (28)$$

$$\ln k_{dp} \propto \frac{(1 - \alpha_{dp}^{ap}) F}{RT}(\phi^d - \phi^d_{1/2}) \quad (29)$$

Whatever the location of the pzc, $(\phi^d - \phi^d_{1/2}) > 0$ for the positive wave and the diffuse layer effect enhances both k_{dp} and k_p upon applying more positive potentials. Conversely, $(\phi^d - \phi^d_{1/2}) < 0$ for the negative wave and the diffuse layer effect inhibits both k_{dp} and k_p upon applying more negative potentials. Since the positive wave shape is mainly determined by the behavior of k_{dp}, whereas k_p controls the negative wave shape, the net effect of the diffuse layer potential is to speed up deprotonation and to slow down protonation.

In the presence of a large surface concentration of acid groups, the value of the diffuse layer potential is dominated by the extent of the ionization process at each potential. Now, the previously discussed trends are reversed (compare the lower panels in Figure 4) and whatever the location of the pzc $(\phi^d - \phi^d_{1/2}) < 0$ for the positive wave, whereas $(\phi^d - \phi^d_{1/2}) > 0$ for the negative wave. As a result, the positive deprotonation wave spreads over a large potential interval, whereas the negative protonation wave becomes much narrower than in the absence of diffuse layer effects.

The electrostatic influence of the external ionized groups ($\Gamma^{ext}_{R\text{-}O^-}$) on the voltammetric response of the buried carboxylic groups ($\Gamma_T^{p/dp}$) is illustrated in Figure S-2 (Supporting Information), which shows that whenever $\Gamma_T^{p/dp}/\Gamma^{ext}_{R\text{-}O^-} \leq 0.1$, ϕ^d remains nearly constant along the voltammogram (i.e., $\phi^d - \phi^d_{1/2} \approx 0$), and the diffuse layer contributions to the protonation/deprotonation kinetics can be neglected, even in the presence of electrolyte at a low concentration.

Comparison with Experiment. Voltammograms associated with a proton exchange between an acidic thiol monolayer and an electrolyte solution display some common characteristics,[17−19] including the presence of reversible anodic and cathodic peaks, a systematic peak potential shift upon varying the solution pH, peak widths at half height close to 90 mV at 298 K, and a bell-shaped variation of the peak intensities with solution pH, which limits the useful pH window to a ∼1 pH unit. All of these characteristics, except for the last one, are reproduced quite well by the theory outlined previously. The inability to account for the peak intensity variation with pH is not likely to be related to any simplification implicit in our model description. In fact, any modeling of a potential-driven proton transfer process under equilibrium conditions is expected to predict a similar wave shift along the potential axis upon varying the solution pH, without introducing significant changes in the peak current. After all, variation of potential and pH are just two alternative ways of influencing protonation energetics.

The origin of the bell-shaped dependence of the peak current on pH can be traced to the evidence provided by Burgess et al.[19] for the presence of a kinetically controlled deactivation process, involving an interaction between the electrolyte cations and the carboxylate groups in the monolayer. This deactivation process results in a lowering of the voltammetric peak intensity at a rate that apparently has a minimum around pH 8.5. Once this deactivation is minimized, by using a low electrolyte concentration and shortening the voltammetric acquisition time, peak intensities become pH independent, at least over a range of two pH units as illustrated in Figure 5a. Then, it suffices to keep the electrode in contact with the solution sufficiently long (e.g., 10^3 s in Figure 5b) to regain the previously reported bell-shaped dependence of the peak intensities on pH (compare parts a and b of Figure 5).

Peak deactivation does not affect greatly the location of the peak potential, and average peak potentials $E_{1/2}$ at low scan rates were recorded over the 6 ≤ pH ≤ 10 range. The slope of the $E_{1/2}$ vs pH plot in Figure 5c has a value of 65 mV/decade, close to the 67 mV/decade reported by Lennox et al.[18] for MUA monolayers and to the 70 mV/decade reported by Burgess et al.[19] for 4-mercaptobenzoic monolayers; in both cases, these monolayers were deposited on polycrystalline gold. Since $E_{1/2} = \phi^m_{1/2} + \Delta\phi^{ref}$, where $\Delta\phi^{ref}$ is a constant term that includes additional potential drops in the measuring circuit, the $E_{1/2}$ vs pH plot can be interpreted on the basis of eq 6. Assuming that the $(\omega_a - 1) \cdot \phi^d_{1/2}/\omega_a$ term does not vary with the solution pH, the slope value gives ω_a = 0.9. Within the framework of the theory described above, this result is

dx.doi.org/10.1021/ac301040r | Anal. Chem. 2012, 84, 5778−5786

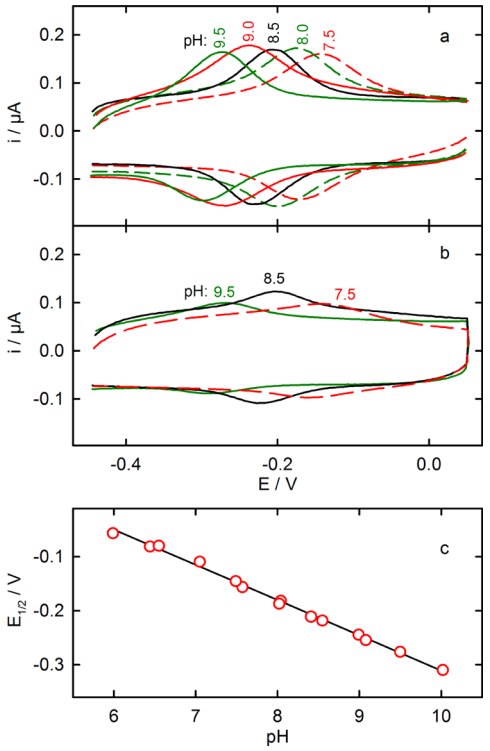

Figure 5. Cyclic voltammograms for a MUA-modified Au(111) electrode in contact with 5 mM NaF solutions of the indicated pH, recorded (a) just after contacting the electrolyte solution or (b) after a delay of 10^3 s. (c) Midpoint potential as a function of solution pH. Scan rate 0.1 V s^{-1}, T = 298 K.

consistent with the observation of narrow voltammetric peaks throughout the explored pH range. The intercept of the plot has a value of 0.34 V vs Ag/AgCl/NaCl (saturated), and it contains the information on the ΔG^0 (or pK_a) value of the acid groups that generate the voltammetric peaks. However, in the absence of reliable estimates of $\Delta\phi^{ref}$ and $\phi^d_{1/2}$, no attempt was made to determine ΔG^0. It is interesting to note that, except for the likely small diffuse layer term, eq 6 predicts $E_{1/2}$ to be independent of the nature of the substrate (and of its pzc), as is the case for MUA deposited on Ag(111),[17] on polycrystalline Au,[18] and on Au(111) in the present work.

A quantitative analysis of the voltammetric response under kinetic control requires a detailed knowledge of the interfacial potential profile, which is often unfeasible. Fortunately, experimental voltammograms are acquired in a pH range where extensive ionization of the acid groups in the monolayer has taken place just after making contact with the electrolyte solution. Moreover, these voltammograms involve only a small charge flow, implying that just a small fraction (typically a few picomoles per cm^2) of the acid groups take part in the potential-driven protonation/deprotonation process. Under these circumstances, two critical approximations can safely be introduced. First, the diffuse layer capacity is likely to be much larger that the monolayer integral capacities, i.e., $C_d \gg K_{md}$, K_{ad}, so that eq 23 can be rewritten approximately as

$$i = K_{md}\nu + \omega_a F\Gamma_T^{p/dp}\frac{d\theta_{R\text{-}O^-}}{dt} \quad (30)$$

Second, the value of ϕ^d is largely determined by the surface concentration of preionized acid groups $\Gamma^{ext}_{R\text{-}O^-}$, and it is not likely to vary along a voltammetric scan. Therefore, $\phi^d - \phi^d_{1/2} \approx 0$, hence $E^c - E^c_{1/2} \approx E - E_{1/2}$, and by inserting these approximations in eqs 15 and 16, eqs 24 and 30 can then be combined to give

$$i = K_{md}\nu + \omega_a F\Gamma_T^{p/dp}k_s^{ap}\exp(-\alpha_M\varphi^2)\exp(\alpha_{dp}^{ap}\varphi) \times[(1-\theta_{R\text{-}O^-}) - \exp(-\omega_a\varphi)\cdot\theta_{R\text{-}O^-}] \quad (31)$$

where $\varphi = F(\phi^m - \phi^m_{1/2})/RT = F(E - E_{1/2})/RT$. Since K_{md}, $E_{1/2}$, and ω_a are determined independently, only the values of $\Gamma_T^{p/dp}$, k_s^{ap}, α_{dp}^{ap}, and α_M are required to fit a given voltammogram to eq 31. These four parameters are related to different voltammetric characteristics. Thus $\Gamma_T^{p/dp}$ and k_s^{ap} determine the area under the voltammetric peaks and their separation, respectively. The shift of the average peak potential with respect to $E_{1/2}$ at high scan rates is governed by the α_{dp}^{ap} value, and α_M affects the shape of the voltammetric peaks when a sufficiently broad range of φ values is explored.

Figure 6 illustrates the adequacy of eq 31 to reproduce the observed voltammetric behavior in a 5 mM NaF solution of pH

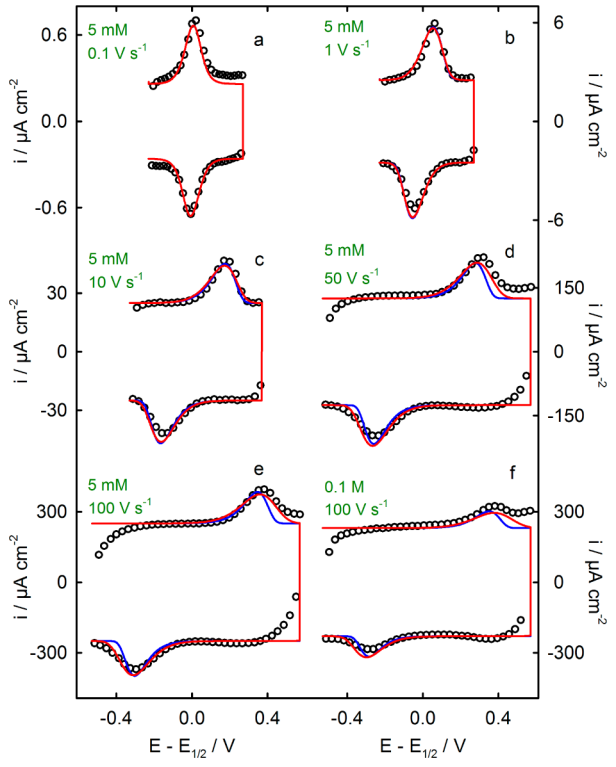

Figure 6. Cyclic voltammograms recorded with a MUA-modified Au(111) electrode in contact with a NaF solution of pH 8.5 at 298 K, as a function of NaF concentration and scan rate (open circles). Solid red lines were computed with eq 31 and the following parameter values: ω_a = 0.9, $E_{1/2}$ = −0.22 V, k_s^{ap} = 10 s^{-1}, α_M = 0.006, α_{dp}^{ap} = 0.43, K_{md} = 2.5 μF cm^{-2}, (a) $\Gamma_T^{p/dp}$ = 5.3 pmol cm^{-2}, (b) $\Gamma_T^{p/dp}$ = 5.0 pmol cm^{-2}, (c) $\Gamma_T^{p/dp}$ = 4.0 pmol cm^{-2}, (d) $\Gamma_T^{p/dp}$ = 4.1 pmol cm^{-2}, (e) $\Gamma_T^{p/dp}$ = 3.3 pmol cm^{-2}, (f) α_{dp}^{ap} = 0.41, K_{md} = 2.3 μF cm^{-2}, $\Gamma_T^{p/dp}$ = 1.9 pmol cm^{-2}. Solid blue lines illustrate the narrower wave shapes that are obtained at high scan rates by setting α_M = 0.

8.5 for scan rates in the range 0.1 V/s ≤ ν ≤ 100 V/s. To assess whether an uncompensated ohmic drop might affect the separation between the voltammetric peaks, Figure 6f shows a voltammogram recorded at 100 V/s in the presence of 0.1 M NaF. By comparing parts e and f of Figure 6, it is evident that the peak separation is independent of the electrolyte

dx.doi.org/10.1021/ac301040r | Anal. Chem. 2012, 84, 5778−5786

concentration, though it is also apparent that the peak area decreases upon increasing the NaF concentration, as expected given the presence of a cation induced deactivation process.[19]

Satisfactory fits are obtained with small $\Gamma_T^{p/dp}$ values, implying that less than one percent of the carboxylic groups in the monolayer are involved in the potential-induced protonation/deprotonation process. These $\Gamma_T^{p/dp}$ values decrease from 5.3 to 3.3 pmol cm^{-2} upon increasing the scan rate, suggesting a distribution of kinetic responses, so that the current contributions from the slowest groups either appear at higher overpotentials or are too small to be distinguished from the background capacitive current. The standard rate constant k_s^{ap} = 10 s^{-1} appears far too low to correspond to a simple proton transfer between two oxygen atoms in close contact. A low value of the rate constant would be expected if neither the OH^- anion nor the H_2O molecule could come in close contact with the buried carboxylic (or carboxylate) groups involved in the potential induced proton transfer, so that the proton should cross a thin layer of entangled hydrocarbon chains to reach its destination. According to eqs 18 and 19, this hypothesis is consistent with an observed $\alpha_{dp}^{ap} = 0.43$, since $\alpha_{dp}^{ap} \approx \alpha_{p}^{ap} \approx \omega_a/2 = 0.45$ would imply $\omega_b \approx 0$ (or $\phi^b \approx \phi^d$), i.e., the proton acceptor and donor from solution would remain at the OHP, while the proton donor and acceptor from the monolayer would stay in the vicinity of the gold surface.

The comparison between experimental and theoretical voltammograms at scan rates ≥50 V s^{-1} (Figure 6d–f) shows that better fits are obtained by including the quadratic potential term in the protonation/deprotonation rate constants. The value of $\alpha_M = 0.006$ that best fits the voltammetric shapes in Figure 6 can be interpreted according to eq 20, by assuming $\omega_a - \omega_b \approx \omega_a = 0.9$, to obtain an upper limit for the reorganization energy of 84 kJ mol^{-1}. This estimate falls within a broad range of values, 30 kJ mol^{-1} < λ < 180 kJ mol^{-1}, previously reported for proton exchange in aprotic solvents.[34,35]

CONCLUSIONS

Our electrostatic analysis of acid thiol monolayers has shown that proton transfer can only produce narrow voltammetric peaks, as experimentally observed, when the immobilized acid groups lie close to the metal substrate. This restriction implies that orientational disorder constitutes a structural prerequisite for observing well developed proton transfer voltammograms. So far, the voltammetric response of carboxy-terminated monolayers has been reported at pH values close to 9, where there is independent evidence for conformational disorder and extensive ionization of the carboxylic groups.[6−13] In agreement with this physical scenario, the small charge recorded under the voltammetric peaks indicates that less than 1% of the carboxylic groups in the monolayer participate in the potential-induced proton transfer process.

By combining a mean-field description of the potential profile with a quadratic relationship between activation energy and electrode potential, a rather simple (though implicit) expression for proton transfer voltammograms with a low concentration of dissociating groups was derived. This expression bears a remarkable similarity with that for a surface attached redox couple, where the number of electrons n is replaced by ω_a, a dielectric parameter related to the location of the reaction site within the monolayer. Quantitative fits of experimental voltammograms at pH 8.5 provide an initial outline of the proton transfer process, in which the interfacial electric field facilitates an intrinsically slow proton exchange between members of a donor−acceptor pair that are not in close contact. Extension of the present approach to the case of a high surface concentration of dissociating groups is currently under way.

ASSOCIATED CONTENT

Supporting Information

Potential profile in the presence of potential-induced deprotonation, experimental details, effect of the potential on the protonation and deprotonation rate constants, derivation of the voltammetric response, and effect of the external carboxylates population on the voltammetric features. This material is available free of charge via the Internet at http://pubs.acs.org.

AUTHOR INFORMATION

Corresponding Author

*Phone: +34-954557177. Fax: +34-954557174. E-mail: fondacab@us.es.

Notes

The authors declare no competing financial interest.

ACKNOWLEDGMENTS

This work was supported by the Spanish MICINN under Grant CTQ2008-00371 and by the Junta de Andalucia under Grant P07-FQM-02492.

REFERENCES

(1) (a) Love, J. C.; Estroff, L. A.; Kriebel, J. K.; Nuzzo, R. G.; Whitesides, G. M. *Chem. Rev.* **2005**, *105*, 1103−1170. (b) Vericat, C.; Vela, M. E.; Benitez, G.; Carro, P.; Salvarezza, R. C. *Chem. Soc. Rev.* **2010**, *39*, 1805−1834.
(2) Wang, G.; Kim, T.; Lee, T. *J. Mater. Chem.* **2011**, *21*, 18117−18136.
(3) Raynor, J. E.; Capadona, J. R.; Collard, D. M.; Petrie, T. E.; García, A. J. *Biointerphases* **2009**, *4*, FA3−FA16.
(4) Frasconi, M.; Mazzei, F.; Ferri, T. *Anal. Bioanal. Chem.* **2010**, *398*, 1545−1564.
(5) Yue, Y.; Waldeck, D. H.; Petrovic, J.; Clark, R. A. *J. Phys. Chem B* **2006**, *110*, 5062−5072.
(6) Smalley, J. F.; Chalfant, K.; Feldberg, S. W.; Nahir, T. M.; Bowden, E. F. *J. Phys. Chem. B* **1999**, *103*, 1676−1685.
(7) Van der Vegte, E. W.; Hadziioannou, G. *Langmuir* **1997**, *13*, 4357−4368.
(8) Vezenov, D. V.; Noy, A.; Rozsnyai, L. F.; Lieber, C. M. *J. Am. Chem. Soc.* **1997**, *119*, 2006−2015.
(9) Ramírez, P.; Granero, A.; Andreu, R.; Cuesta, A.; Mulder, W. H.; Calvente, J. J. *Electrochem. Commun.* **2008**, *10*, 1548−1550.
(10) Dai, Z.; Ju, X. *Phys. Chem. Chem. Phys.* **2001**, *3*, 3769−3773.
(11) Kakiuchi, T.; Iida, M.; Imabayashi, S.; Niki, K. *Langmuir* **2000**, *16*, 5397−5401.
(12) Fears, K. P.; Creager, S. E.; Latour, R. A. *Langmuir* **2008**, *24*, 837−843.
(13) (a) Gershevitz, O.; Sukenik, C. N. *J. Am. Chem. Soc.* **2004**, *126*, 482−483. (b) Gershevitz, O.; Osnis, A.; Sukenik, C. N. *Israel J. Chem.* **2005**, *45*, 321−336.
(14) Bryant, M. A.; Crooks, R. M. *Langmuir* **1993**, *9*, 385−387.
(15) Wang, J.; Ward, M. D.; Ebersole, R. C.; Foss, R. P. *Anal. Chem.* **1993**, *65*, 2553−2562.
(16) Dai, Z.; Ju, X. *Phys. Chem. Chem. Phys.* **2001**, *3*, 3769−3773.
(17) White, H. S.; Peterson, J. D.; Cui, Q.; Stevenson, K. J. *J. Phys. Chem. B* **1998**, *102*, 2930−2934.
(18) Burgess, I.; Seivewright, B.; Lennox, B. R. *Langmuir* **2006**, *22*, 4420−4428.
(19) Rosendahl, S. M.; Burgess, I. J. *Electrochim. Acta* **2008**, *53*, 6759−6767.

(20) Chen, Y.; Yang, X.; Jin, B.; Guo, L.; Zheng, L.; Xia, X. *J. Phys. Chem. C* **2009**, *113*, 4515−4521.
(21) Smith, C. P.; White, H. S. *Langmuir* **1993**, *9*, 1−3.
(22) Fawcett, W. R.; Fedurco, M.; Kovacova, Z. *Langmuir* **1994**, *10*, 2403−2408.
(23) Andreu, R.; Fawcett, W. R. *J. Phys. Chem.* **1994**, *98*, 12753−12758.
(24) Schreiber, F. *Prog. Surf. Sci.* **2000**, *65*, 151−256.
(25) Capitán, M. J.; Alvarez, J.; Calvente, J. J.; Andreu, R. *Angew. Chem., Int. Ed.* **2006**, *45*, 6166−6169.
(26) Osnis, A.; Sukenik, C. N.; Major, D. T. *J. Phys. Chem. C* **2012**, *116*, 770−782.
(27) Krishtalik, L. I. *Biochim. Biophys. Acta* **2000**, *1458*, 6−27.
(28) Kiefer, P. M.; Hynes, J. T. *J. Phys. Org. Chem.* **2010**, *23*, 632−646.
(29) Kuznetsov, A. M.; Ulstrup, J. *J. Phys. Org. Chem.* **2010**, *23*, 647−659.
(30) Kiefer, P. M.; Hynes, J. T. *Solid State Ionics* **2004**, *168*, 219−224.
(31) Kiefer, P. M.; Hynes, J. T. *J. Phys. Chem. A* **2002**, *106*, 1834−1849.
(32) Kiefer, P. M.; Hynes, J. T. *J. Phys. Chem. A* **2004**, *108*, 11793−11808.
(33) Bard, A. J.; Faulkner, L. R. *Electrochemical Methods*; J. Wiley: New York, 2001; Chapter 14.
(34) Goez, M.; Heun., R. *Angew. Chem., Int. Ed.* **1998**, *37*, 3052−3054.
(35) Heeb, L. R.; Peters, K. S. *J. Phys. Chem. A* **2006**, *110*, 6408−6414.